Laser wakefield acceleration of electrons using high-order Bessel-Gauss beams for driver beam and electron bunch guiding

Vidmantas Tomkus (vidmantas.tomkus@ftmc.lt)
State research institute Center for Physical Sciences and Technology
Valdas Girdauskas
State research institute Center for Physical Sciences and Technology
Mehdi Abedi-Varaki
State research institute Center for Physical Sciences and Technology
Gediminas Račiukaitis
State research institute Center for Physical Sciences and Technology

Article

Keywords:

Posted Date: April 20th, 2022

DOI: https://doi.org/10.21203/rs.3.rs-1561509/v1

Laser wakefield acceleration of electrons using high-order Bessel-Gauss beams for driver beam and electron bunch guiding

VIDMANTAS TOMKUS[1*], VALDAS GIRDAUSKAS[1,2], MEHDI ABEDI-VARAKI[1], AND GEDIMINAS RACIUKAITIS[1]

[1]*Center for Physical Sciences and Technology, 231 Savanoriu Ave., LT-02300, Vilnius, Lithuania*
[2] *Vytautas Magnus University, K.Donelaicio St.58, LT-44248, Kaunas, Lithuania*
* *vidmantas.tomkus@ftmc.lt*

Abstract: High-intensity laser pulse propagating through a gas target disturbs uniform plasma distribution. Plasma density structures, created by high-order Bessel-Gauss beams for guiding the Gaussian beam driver and laser wakefield acceleration of electrons, are analysed using Wake-T and Fourier-Bessel Particle-In-Cell (FBPIC) simulation tool. The utilisation of Bessel-Gauss beams increases the acceleration distance and energy of accelerated electrons up to 50% relative to the Gaussian beam of the same intensity.

1. Introduction

Studies on the interactions of laser radiation with plasma, after the advent of the laser chirped pulse amplification (CPA) technique and increased interest in high-peak-power femtosecond (fs) and terawatt-class lasers with a wide range of their applications, are an exciting area of research. The propagation of these laser pulses over a long distance and the ability to create a plasma channel and control its length are significant subjects for laser wakefield accelerators (LWFA)[1,2], and inertial confinement fusion (ICF)[3]. The guiding methods developed can be divided into three categories: 1) self-focused propagation, 2) hollow fibre structures, and 3) pre-formed plasma waveguide. The first method is associated with relativistic self-focusing and ponderomotive charge displacement by the fs (or TW) laser pulse. Indeed, by employing this method, the refractive index of the on-axis plasma increases with the relativistic increase of electron inertia near the centre of the beam or by ponderomotive charge expulsion[4]. In addition, the plasma channel generated by guiding fs laser pulses depends on the interaction length (which is usually limited to the Rayleigh length) and has diverse applications in remote sensing[5,6], terahertz radiation generation (THz)[7,8], high harmonic generation[9], and X-ray lasers[10].

Furthermore, using plasma densities that facilitate self-focusing of the laser pulse in an ionised gas, guiding a short laser pulse beyond its Rayleigh length can be achieved. However, these processes typically are delicate to plasma instabilities[11]. However, stable plasma guiding techniques have illustrated that it is possible to produce plasma channels and accelerate electron bunches up to 8 GeV. These techniques are related to the application of a capillary discharge inside a gas target and, in combination with a laser heater that leads to the creation of a parabolic plasma channel guiding subsequently an additional driving high-peak-power laser pulse over about 10 cm[12,13]. Another promising method is using an axicon lens and a femtosecond laser beam to release energy into the elongated focus area and finally produce plasma channels[14]. Many experimental and theoretical investigations for guided laser beam propagation have demonstrated that owing to the recombination process, the lifetime of a plasma channel created by a single fs laser pulse is several nanoseconds[15]. It would be better to mention that employing a long pulse with inverse Bremsstrahlung to heat the plasma electrons leads to prolonging the channel lifetime[16]. Although, long pulses, due to diffraction losses, are challenging to propagate over long distances. It is extremely challenging to cope with all of these conditions for a single guiding scheme.

Nevertheless, relativistic and ponderomotive self-channelling is a unique method to do that[17]. Lately, plasma channels produced by various techniques have been studied by several scholars. Lu et al.[18] considered the Quasi-steady-state air plasma channel produced by a unique fs-laser source. They have shown that a plasma channel with a 60-80 ns lifetime was formed by such pulse sequences in air. Smartsev et al.[19] presented axiparabola as a novel reflective optics instrument that permits prolonging the generation of diffraction-free beams to high-peak-power and broadband laser pulses. It was observed that a laser beam shaped by axiparabola generates a 10 mm plasma channel and guides a 20 TW laser radiation over nearly 10 Rayleigh lengths. Shalloo et al.[20] showed that fully-ionised and low-density plasma channels could be produced by the hydrodynamic expansion of plasma columns generated by optical field ionisation (OFI). Furthermore,

it was found that an axicon lens could be used to generate long plasma channels with on-axis densities on the order of $n_e \approx 10^{17}$ cm^{-3}, matched spot-sizes $W_M \approx 40$ μm, and attenuation lengths of order $L_{att} \sim 1000$ mm. Lemos et al.[21] explored that plasma waveguides produced with ultra-short laser pulses in gas jets can guide high-intensity laser pulses. They have guided the laser pulses with intensities ~10^{15} Wcm^{-2} in an 8 mm long hydrogen plasma waveguide with a 35% guiding efficiency.

Zhang et al.[22] investigated the electron beam acceleration with multiple transverse plasma density structures in a wakefield driven by a Laguerre-Gauss (LG) pulse through three-dimensional PIC simulations. It was found that the wakefield has various transverse structures under proper conditions, and it was demonstrated that the doughnut-like wakefield structures could accelerate the ring-shaped hollow electrons beam. Tang et al.[23] studied the propagation dynamics of the azimuthally-polarised first-order Bessel–Gauss (BG) laser beam in a parabolic plasma channel by using a two-dimensional PIC simulation. It was observed that the evolution of this dark hollow laser beam during propagation in the plasma channel could be classified into three types: 1) the propagation with a constant ring-shaped beam radius and width, 2) the synchronous periodic defocusing oscillation, 3) the synchronous periodic focusing oscillation. Vieira and Mendonça[24] considered the nonlinear laser-driven doughnut wakefields for positron and electron acceleration. They have shown that nonlinear wakefields driven by LG laser pulses can lead to the self-injection of ring-shaped electron bunch and positron acceleration. In addition, it was seen that high-order modes of the laser beam could drive doughnut-shaped blowout wakefields with strong positron accelerating gradients similar to those of a spherical bubble. Osterhoff et al.[25] generated laser-driven, low-divergence electron beams of up to about 200 MeV from the steady-state-flow gas cells. It was concluded that LWFA of this kind provides an excellent source of relativistic electrons appropriate for many applications like the production of extreme-ultraviolet undulator radiation. Geddes et al.[26] studied plasma density gradient injection of low absolute momentum spread in electron bunches. It was perceived that the electron bunches could be employed as an injector to a wakefield accelerator to generate stable beams with 0.2 MeV/c-class momenta spread at high energies.

This paper aims to study the effects of driver pulse guiding provided by a doughnut Bessel-Gauss beam for wakefield particle acceleration by using the PIC simulation method. The research is pushed by the progress in high-intensity, high-repetition-rate OPCPA lasers[27], which seem to be a promising alternative for LWFA applications to conventional but limited in performance Ti-sapphire lasers with >30 fs pulse durations and a few Joule pulse energies. These emerging kHz-class lasers typically operate at a lower pulse energy of tens of millijoules and have a pulse duration of 7-10 fs. To drive the charged particles using this type of laser in LWFA self-guiding bubble regime, plasma concentrations of n=3-5×10^{19} cm^{-3} are required[28]. Consequently, the plasma bubble reduces from the typical 25 μm to 8 μm. Tighter focusing of the laser beam is required. It leads to shorter acceleration distances of hundreds of micrometres, relatively low energy and high energy spread of accelerated electrons. Lowering the plasma concentration down to n= 3×10^{18} cm^{-3} would increase the acceleration distance. However, the available laser pulse energy of 40-60 mJ focused to the laser beam waist of 7-8 μm allows reaching the intensities with the laser strength parameter a_0=1.5-2 only. The laser beam propagation is no longer in a self-guiding regime, and additional means for extending acceleration distance are required. Increasing the acceleration distance with the suppressed leak of laser energy permits getting high-energy electron bunches with a low energy spread and divergence. The ultimate goal of the LWFA research is to get stable electron bunches at a high repetition rate for very high energy electron (VHEE) radiotherapy[29-31].

Advances in laser beam shaping permit getting nearly any desired spatial-temporal distribution of laser energy, and we performed detailed simulations on the interaction of a plasma target with combined doughnut-shaped and Gaussian laser pulses with a delay between laser pulses in a femtosecond time scale. In this article, we investigate plasma structures excited by the Bessel-Gauss doughnut beam for guiding the Gaussian driver beam and laser wakefield acceleration of electrons using the Wake-T and FB-PIC simulation tools.

2. Driver beam guiding using a high-order Bessel-Gauss beam

2.1 Dynamic plasma channel for guiding the drive beam

The simulation was performed using the first and second-order Bessel-Gauss (BG) beams to understand the influence of the transverse laser beam intensity profile on plasma density distribution and optical and electron beam guiding. Wake-T simulation results in Fig. 1 show that when a high-intensity ($a_{0b} > 1$) BG beam propagates in a sub-critical concentration plasma, and ring-shaped, high electron concentration zones are formed in the plasma, and they are moving with the plasma wave.

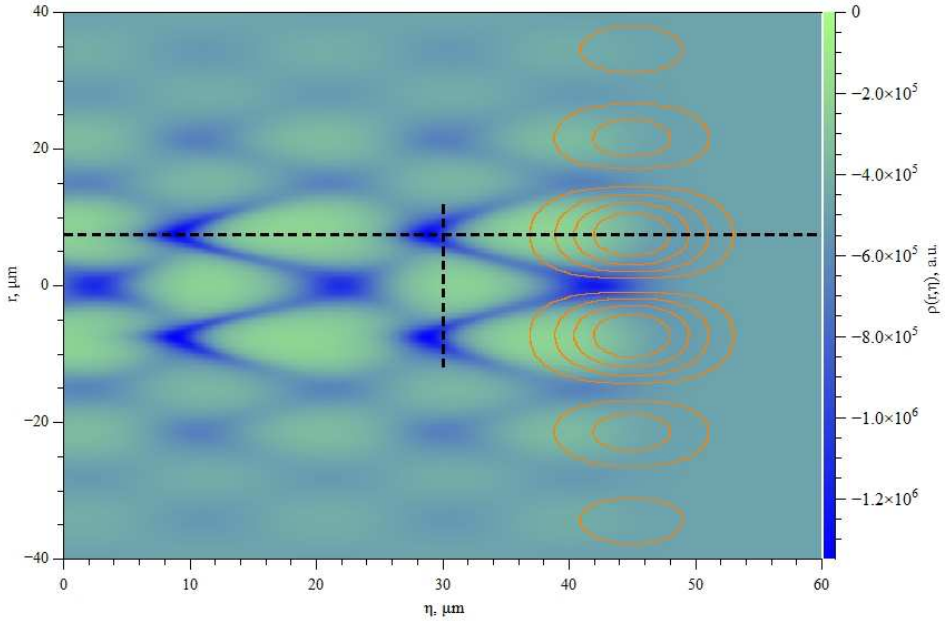

Fig. 1. Electron charge density distribution ρ(r, η) in BG created plasma wave (green-blue) and the first-order BG pulse envelope (isolines). Dotted lines mark the positions of longitudinal and transverse cross-sections of charge density profiles shown in Fig. 2 and Fig. 3. Plasma electron concentration $n_0=3\times10^{18}cm^{-3}$, BG pulse parameters: $a_{0b}=1.5$, $\tau_b=25$ fs, $w_{0b}=7.5$ μm. The laser pulse propagates from the left to right side along the z-axis, centred at r=0.

The transverse charge density profiles of the plasma are shown in Fig. 2. The difference in charge density on the z-axis and at the plasma ring highly depends on the laser beam strength parameter a_0. For higher intensity BG pulse, we could expect the more expressed effect of the plasma ring to the accelerating driver laser pulse and electron bunch propagation.

The transverse charge density distribution, presented in Fig. 2, shows that the charge density profile for the first-order Bessel-Gauss beam (B_1G) near the beam propagation axis at a selected point on the z-axis is close to parabolic (Fig. 2a). Another laser pulse or electron bunch placed at that position along the z-axis could feel like being in a channel as the whole structure moves at the speed of light. Therefore, we can expect that the ring-shaped electron concentration distribution moving with the plasma wave can act as a plasma channel[12,13] for guiding the accelerating laser pulse, maintaining its high peak intensity and accelerating injected electron bunch. The transverse profile of the plasma distribution produced by the second-order Bessel-Gauss beam (B_2G) differs significantly from parabolic (Fig. 2b). However, even with that plasma density profile, we observe an excellent guiding effect (Fig. 6b). If the laser strength parameter a_{0b} increases from 1 to 1.6, the maximum negative charge density in the ring increases from 3 to more than 7 times the initial plasma density, facilitating better waveguiding properties of the ring-shaped plasma structure.

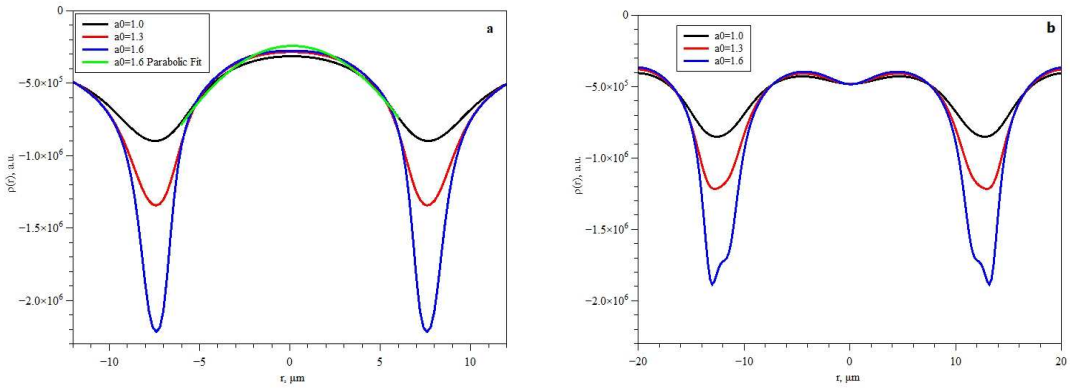

Fig. 2 Transverse profiles of electron charge density ρ(r) for first-order (a) and second-order (b) BG pulses and various values of the laser strength parameter a_{0b}. The green line in (a) is a parabolic approximation. Plasma electron concentration $n_0=3\times10^{18}cm^{-3}$, BG pulse parameters: $\tau_b=25$ fs, $w_{0b}=7.5$ μm.

This waveguide exists only for a limited distance along the beam propagation direction, and we performed a detailed simulation on the guiding effect of the plasma electrons ring to the Gaussian laser pulse. The longitudinal charge density profiles of Fig. 3, along the dotted line shown in Fig. 1, show that the axial length of the annular high electron concentration zone is about 6 μm, and it decreases slightly with the increasing a_{0b} parameter of the BG beam.

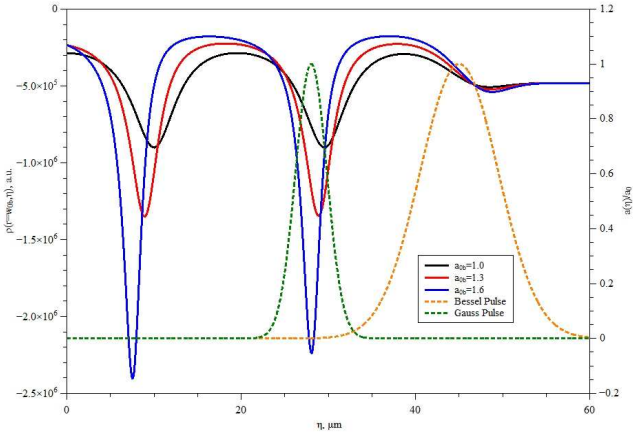

Fig. 3. Longitudinal profiles of the electron charge density ρ (η) for various laser strength parameter values a_{0b} of the BG pulse (solid lines) and normalised envelopes of the accelerating Gaussian (green) and BG pulses (yellow). Plasma electron concentration $n_0=3\times10^{18}cm^{-3}$; Gaussian pulse duration $\tau=10$ fs; BG pulse parameters: $\tau_b=25$ fs, $w_{0b}=7.5$ μm.

To ensure the waveguiding effect of the plasma channel over the entire length of the accelerating laser pulse (green dotted line in Fig. 3), the accelerating pulse should fit inside the high-concentration electron ring (dip). Its spatial spread along the propagation direction should be short enough to avoid diffraction losses of energy on the tails of the pulse. In addition, as the group velocity of the BG pulse differs from the accelerating Gaussian pulse, the spatial duration of the accelerating pulse should be less than the axial length of the electron ring. Therefore, a 10 fs long Gaussian pulse was used to drive the acceleration, while the guiding BG pulse was selected to be 25 fs long. Technically that could be implemented by transmitting part of the Gaussian beam with a pulse duration of 10 fs through a transparent phase mask, which not only transforms the beam to Bessel-Gauss but also extends its duration due to dispersion in the bulk.

The Wake-T simulation results also showed that the maximum density of the negative charge in the electron ring depends on the BG pulse duration and the initial plasma electron concentration (Fig. 4).

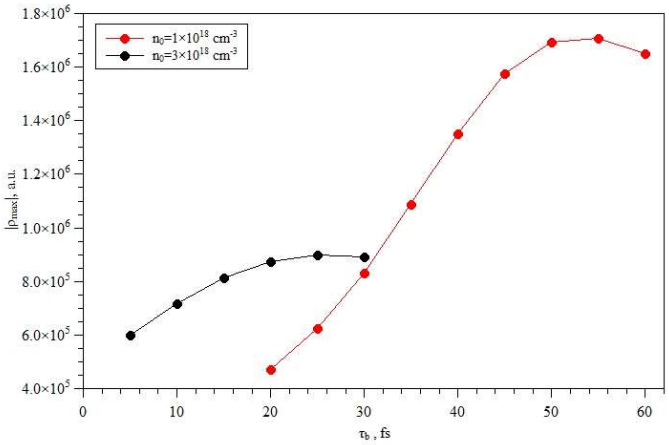

Fig. 4. Dependence of the maximum charge density in the ring-shaped electron plasma wave created by the BG laser pulse on its duration for two different initial plasma electron concentrations: $n_0=1\times10^{18}cm^{-3}$, $n_0=3\times10^{18}cm^{-3}$. BG pulse parameters: $a_{0b}=1.5$, $\tau_b=25$ fs, $w_{0b}=7.5$ μm.

With decreasing plasma concentration, the maximum value of charge density in the ring "waveguide cladding") is reached for longer BG pulse durations. For $a_{0b}=1.0$, the pulse duration, at which the charge density value is the highest, increases from 25 fs to 55 fs when the initial plasma concentration decreases from 3×10^{18} cm^{-3} to $n_0=1\times10^{18}$ cm^{-3}. A particularly strong dependence of the maximum charge density on the pulse duration is observed for lower plasma concentrations. Based on those results, 25 fs pulse duration was selected for the guiding BG pulses in our simulations.

2.2 Guiding the driving Gaussian beam by the plasma ring

Simulating the accelerating pulse propagation in the plasma perturbed by the BG pulse, the initial value of the pulse peak coordinate z_c was adjusted to the first dip in the longitudinal charge density profile, corresponding to the high-concentration electron plasma ring (Fig. 2), and the spatial pulse duration was selected to equal to $c\tau = 3\ \mu m$ to fit within the dip in the charge density profile (Fig. 5).

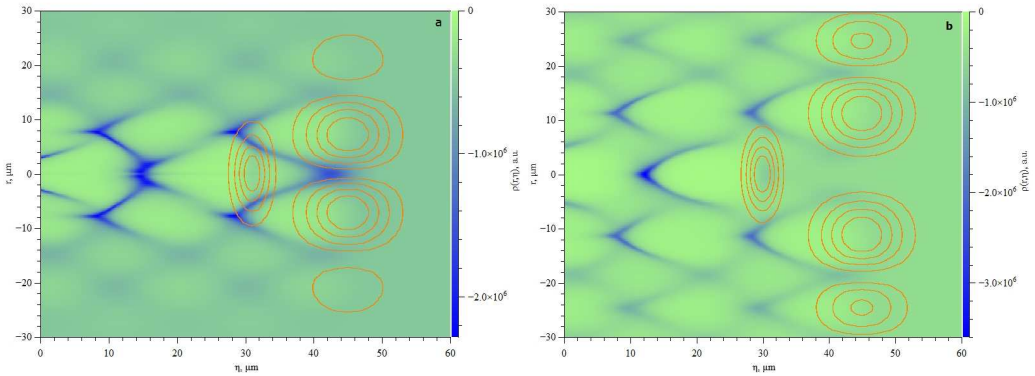

a) b)

Fig. 5. Electron charge density distribution ρ(r, η) in the plasma wave (green-blue) and the envelopes (isolines) of the accelerating Gaussian pulse and pulses of B_1G (a) B_2G (b) beams. Parameters of the accelerating Gaussian and BG pulses: a_0=2.0, τ=10 fs, w_0=7 μm, a_{0b}=1.5, τ_b=25 fs, w_{0b}=7.5 μm (a); w_{0b}=11 μm (b).

The simulation results show that the guiding effect on the propagation of the accelerating pulse in the BG pulse plasma wake is evident as the central part of the accelerating beam maintains an almost constant diameter at a distance 10 and more times the Rayleigh length of the beam $z_R = \pi w_0/\lambda$ (Fig. 6).

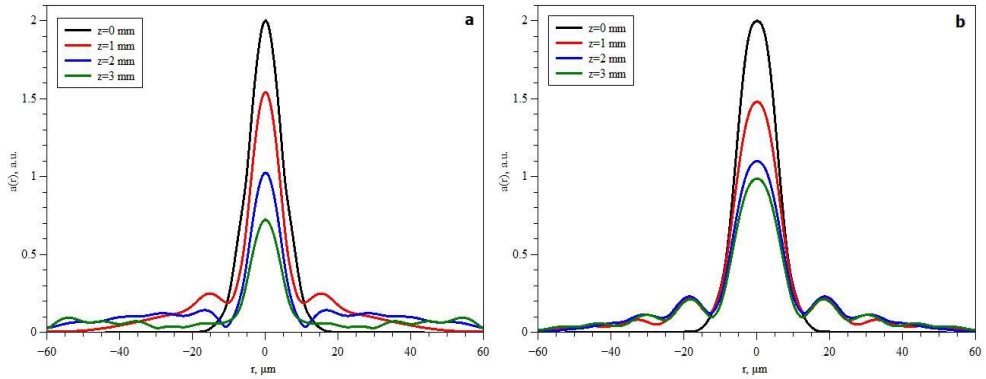

Fig. 6. Transverse profiles a(r) of the accelerating pulse amplitude at the pulse peak, guided by the first-order (a) and second-order (b) BG pulses at various propagation distances in plasma (0, 1, 2, 3 mm). Parameters of the accelerating Gaussian and BG pulses: a_0=2.0, τ=10 fs, w_0=7 μm, a_{0b}=1.5, τ_b=25 fs, w_{0b}=7.5 μm.

However, the maximum amplitude decreases with the propagation distance due to the leak of laser energy through "soft waveguide cladding" and the difference in the group velocity of the accelerating pulse from the group velocity of the BG pulse. At the initial propagation distance (<0.4 mm), the mode size corresponding to the profile of the moving plasma waveguide is formed, which depends on the ratio w_0/w_b of the initial radius of the accelerating beam to the radius of the doughnut BG beam. When the propagation distance exceeds $\sim 10z_R$, the modulation of the temporal envelope of the pulse begins to become apparent. For the distance exceeding $\sim 20z_R$ (~2 mm), the laser pulse is decomposed into several pulses separated in time, and the maximum laser intensity falls significantly. Therefore, we have limited acceleration distance.

3. Electron acceleration using a higher-order Bessel-Gauss beam

Based on the initial simulation results of 2D quasi-static PIC code Wake-T, the more advanced FBPIC code was used to model laser wakefield acceleration of electrons using higher-order Bessel-Gauss beams. B_1G and B_2G cases were

modelled. As a probe, a Gaussian electron bunch with a charge of 1 pC, a standard deviation of $\sigma_{r,z}$ = 1 μm in longitudinal and transversal direction, the relative electron energy spread of 5%, and initial energy of 10 MeV was injected at the position of the maximum of the longitudinal electric field E_z of the plasma wave. The duration of the accelerating Gaussian laser pulse of τ = 10 fs (the spatial duration equal to $c\tau = 3\ \mu m$) was chosen to fit the width of the plasma structures created by the guiding Bessel-Gauss beam (Fig. 3). The Gaussian beam radius of w_0 =7 μm was matched to the radius of the first ring of w_b = 7.5 μm for the B_1G beam, and w_b = 11 μm for the B_2G beam. The laser strength parameter of a_{0b} = 1.5 was used based on the Wake-T simulation results (Fig. 1-4). The duration of the guiding Bessel-Gauss beam of τ_b = 25 fs and the initial concentration of electrons in plasma $n_0 = 3\times10^{18}$ cm^{-3} were selected based on the maximal charge density in the plasma ring excited by the BG beam (Fig. 4). The maximum acceleration distance in plasma was L = 3 mm, and the divergence of the electron bunch θ_E was defined as an average of $\theta_{Ex,y}=2\cdot arctan(u_{x,y}/u_z)$ in x and y directions, where u_x, u_y and u_z are normalised electron momenta in the directions of x, y and, z.

The results of the FBPIC simulation for the Gaussian (G), Gaussian combined with B_2G (G+B_2G), Gaussian combined with B_1G (G+B_1G), and B_1G laser beam configurations are shown in Fig. 7. The highest energy of accelerated electrons with a moderate energy spread and the electron beam divergence were obtained using a Gaussian beam with the laser strength parameter of a_0 = 5.0, guided by the B_2G beam with a_{0b} =1.5 (G+B_2G configuration). For that laser strength parameter, the maximum energy of accelerated electrons reached 244 MeV (Fig. 7a), and there was no saturation in the energy ramp at the 2 mm acceleration distance. The energy spread for this configuration was close to 30% (Fig. 7b), and the minimum divergence was 27 mrad. (Fig. 7c). The energy spread stabilises after 0.5 mm of acceleration, and divergence is improving with the distance.

Application only of the Gaussian beam with the same strength parameter a_0 = (5.0 + 1.5) = 6.5 is more efficient in LWFA at short acceleration distances. However, the substantial divergence of the focused Gaussian beam after the waist leads to a reduction of intensity (a_0). The guided Gaussian beam in the G+B_2G configuration preserves its strength parameter over a longer distance (Fig. 7d).

Guiding the Gaussian beam by the first-order Bessel-Gauss beam (G+B_1G) was not efficient because of the interference of the axial longitudinal electric field of the Gaussian and B_1G beams (Fig. 7a,b,c).

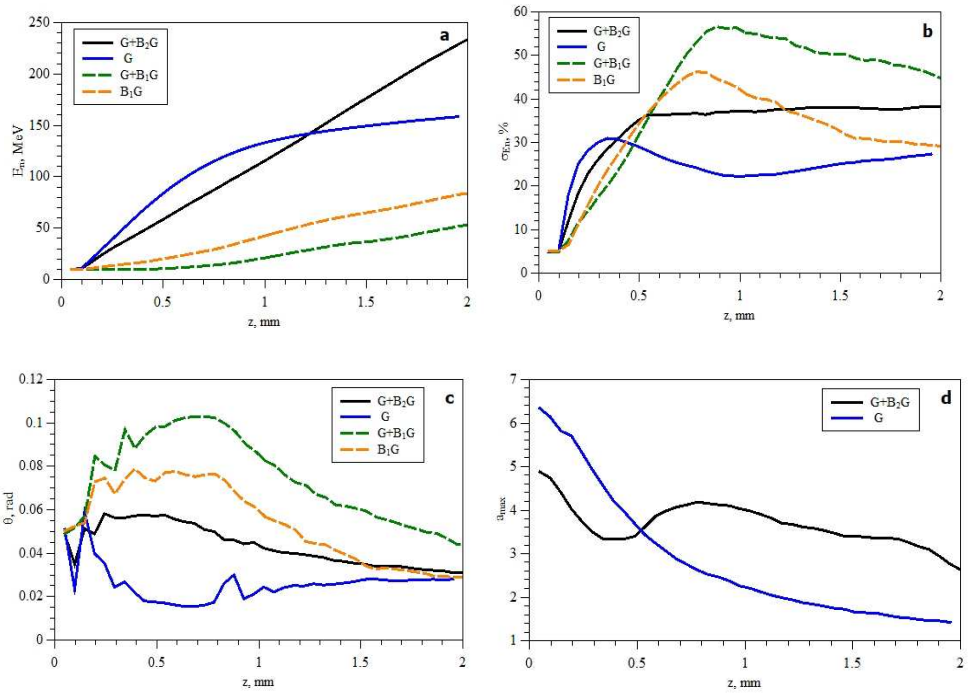

Fig. 7. Dependence of the energy of accelerated electrons (a), energy spread σ_{En} (b), divergence θ_E (c), and driver pulse amplitude (d) on the acceleration distance for Gaussian (G), Gaussian and B_2G (G+B_2G), Gaussian and B_1G (G+B_1G) and B_1G (B_1G) laser beams. Parameters of the accelerating Gaussian and Bessel-Gauss beams: τ=10 fs, w_0=7 μm, a_{0b}=1.5, τ_b=25 fs, w_{0b}=7.5 μm and a_{0b}=1.3 for B_1G, w_{0b}=11 μm and a_{0b}=1.5 for B_2G, a_0=6 for G; a_0=5 for G+B_2G, a_0=1.5 for G+B_1G.

For all values of the parameter a_0 presented in Fig. 7, the effective acceleration takes place up to the distance of z ~ 2-3 mm. For longer distances, the energy growth slows down significantly or stops growing. Because of the nonlinear phase modulation of the accelerating pulse (nonlinear chirp), the laser beam splits into several beamlets, and the amplitude of the central accelerating peak is reduced significantly.

In Fig. 8-Fig. 11and Table 1, the results of the FBPIC LWFA simulation and characteristics of the accelerated 1 pC Gaussian electron bunch at the distance of 2 mm, using three different laser beam configurations, are presented. For comparison, LWFA using the Gaussian beam, the Gaussian beam guided by the B_2G beam, and LWFA using a B_1G beam only were investigated. The laser strength parameters and pulse durations of the beams are presented in Table 1.

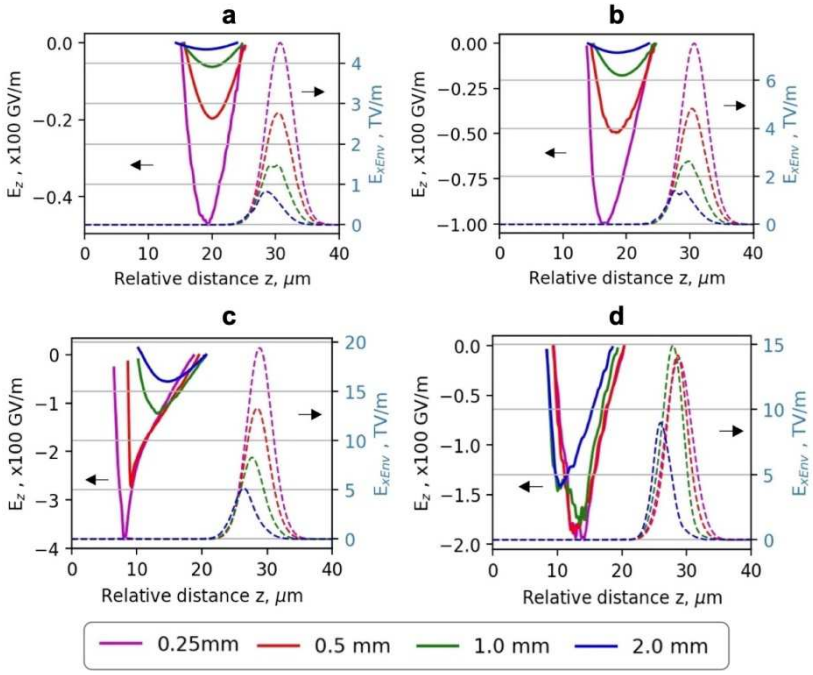

Fig. 8. Dependence of the longitudinal plasma wake electric field E_z (solid line) and the electric field of laser beam envelope (dotted line) for acceleration distances 0.25 mm, 0.5 mm, 1 mm, 2 mm of the Gaussian beam with the laser strength parameter a_0=1.9 (a), a_0=3.0 (b), a_0=6.5 (c) and the Gaussian beam with a_0=5.0 guided by the B_2G beam with a_0=1.5 (G+B_2G) (d).

The intensity of the Gaussian beam and corresponding plasma wake (GV/m) fall down rapidly with the propagation distance. That is due to strong diffraction of the Gaussian beam after the waist due to a short Rayleigh length for a tight, focused Gaussian beam (Fig. 8a,b,c). The waist radius of the laser beam increases from 7 μm to 50 μm for a_0 = 1.9 and to 24 μm for a_0 = 6.5 (Fig. 9a,c). The diffraction is opposed by non-linear self-guiding intensive laser beams. With increasing the intensity of the Gaussian beam from a_0 = 1.9 to a_0 = 6.5, the self-guided propagation becomes more visible.

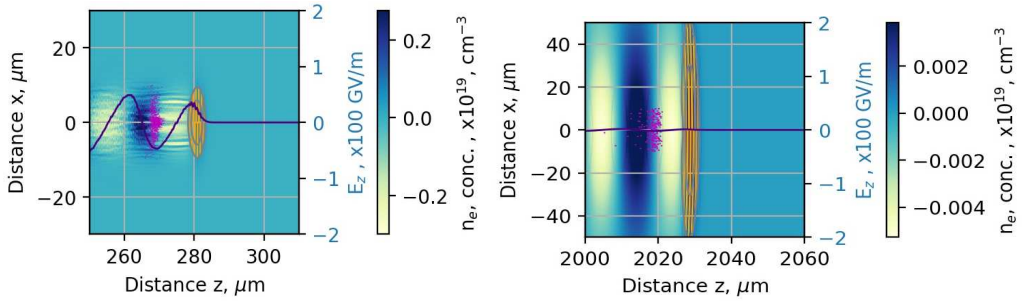

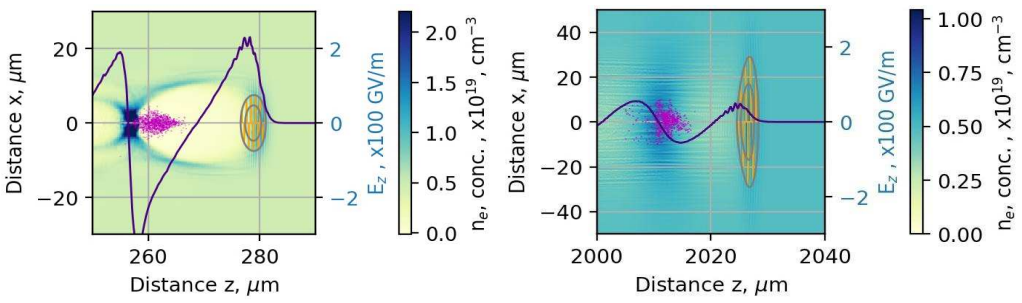

Fig. 9. Distribution of plasma concentration (colour map) and longitudinal plasma wake electric field E_z (line) formed along a beam axis by the Gaussian beam with the laser strength parameter a_0=1.9 (a,b) and a_0=6.5 (c,d). Isolines and yellow oscillating lines represent the location and intensity of the electrical field of the laser pulse. The violet cloud is the electron bunch injected behind the laser pulse.

The initial value of the laser strength parameter a_0 affects the strength of longitudinal electrical field E_z, responsible for the acceleration of electrons by the wake. By increasing the acceleration distance from 0.25 mm to 0.5 mm for a_0 = 1.9, the electric field of the laser beam envelope drops from 4.5 TV/m to 2.8 TV/m and to 0.9 TV/m at a distance of 2 mm. The longitudinal electric field of the plasma wake drops from 48 GV/m to 20 GV/m and to 10 GV/m at distances of 0.25 mm, 0.5 mm and 2 mm, correspondingly (Fig. 8a, Fig. 9a,b). The weighted mean energy of the accelerated electron bunch reaches 28±7 MeV, and the divergence θ_E =41 mrad (Table 1).

The wake is shifted back relative to the driving laser pulse in the case of a more intensive laser pulse, indicating the increase in plasma bubble size. The radius of the plasma bubble increases proportionally to $(a_0)^{1/2}$ allowing a higher acceleration distance of electrons. At the distances from 0.25 mm to 0.5 mm for a_0 = 6.5, the electric field of the laser beam envelope drops from 19 TV/m to 13 TV/m and to 5 TV/m at 2 mm (Fig. 8c, Fig. 9c,d). Compared to the a_0 = 1.9, the decrease of laser intensity at a distance from 0.25 mm to 2 mm is 30% lower. The longitudinal electric field of the plasma wake drops from 380 GV/m to 280 GV/m and to 50 GV/m at the distances 0.2of 5 mm, 0.5e mm and 2 mm, correspondingly.

At the initial acceleration distance from 0.25 mm to 0.5 mm, the nonlinear expansion of the bubble radius reduces the drop of the longitudinal electric field by 78% relative to the a_0 = 1.9 case. The minimum of the longitudinal electric field shifts 1.8 times further from the driving beam position increasing the dephasing distance of accelerated electrons. The electrons are accelerated up to 159±44 MeV, and the divergence θ_E =27 mrad (Fig. 11a and Table 1).

For the G+B_2G configuration with a combined laser strength parameter a_0=5.0+1.5 = 6.5, equal to the Fig. 8c case, the plasma wake preserves a high accelerating field E_z at the 2.0 mm distance (Fig. 8d). That is clear evidence of the positive guiding effect of the Gaussian beam by the plasma ring produced by the BG beam.

The longitudinal electric field of the plasma wake in the central part of the B_2G beam is low, of the order of 10 GV/m, and is formed by the guided Gaussian beam. The electric field of the Gaussian beam envelope remains almost constant at a distance from 0.25 mm to 0.5 mm and drops from 14 TV/m to 9 TV/m at 2 mm (Fig. 8d, Fig. 10a,b). The longitudinal electric field of the plasma wake is at the level of 180 GV/m at a distance from 0.25 mm to 0.5 mm and drops to 130 GV/m at 2 mm. Compared to the Gaussian beam with a_0 = 6.5, the absolute values of the laser intensity and longitudinal electric field at the distance of 0.25 mm are 1.4-2.1 times lower. However, the electric fields of the laser beam and plasma wake at 2 mm are by factors of 2.1 and 2.6, correspondingly higher. The electrons are accelerated at a 53% higher energy of 244±83 MeV with the divergence θ_E =27 mrad (Fig. 11b and Table 1).

In Fig. 10cd, the LWFA simulation results using the B_1G beam are shown. The waist radius of the B_1G beam almost does not change within the distance of 2 mm. The waist radius of 7.5 μm was chosen to form a relevant distribution of the plasma concentration in the central part of the doughnut B_1G beam. Depending on the waist radius and concentration, the intersecting plasma waves of the ring beam form a plasma bubble with a diameter close to the plasma wavelength. The emerging longitudinal electric field inside the central part of the bubble varies slowly within the acceleration distance of 2 mm. For a_0 = 1.3, 1.9, and 3.0, the longitudinal electric field of the plasma wake is in the range of 15-25 GV/m, 50-90 GV/m, and 100-150 GV/m, correspondingly (Fig. 10c,d). The constant acceleration of the electron bunch allows it to reach the 3-4 times higher mean electron energy of 38±20 MeV, 121±38 MeV, and 149±42 MeV, correspondingly, relative to the Gaussian beam with the same laser intensity a_0 (Table 1). The formation of the Bessel-

Gauss beam requires, however, higher pulse energy compared to the Gauss beam because of the energy allocated in the Bessel rings and distributed within the acceleration distance of 2 mm.

With increasing the laser strength parameter up to a_0 = 5.0, the expanding blow-out area of the doughnut Bessel-Gauss beam ring changes the structure of interfering plasma waves. It results in a longitudinal electric field varying in the range of 20-140 GV/m. The weighted mean energy of the accelerated electron bunch starts to drop down to 141±25 MeV. Compared to the Gaussian beam, the highest gain of the energy of the accelerated electrons is reached at the lower laser intensities with a_0 =1.3-1.9. The divergence of θ_E =41 mrad is high for the a_0 =1.3 and remains in the range of θ_E =21-23 mrad for the a_0 =1.9, a_0 =3.0 and a_0 =5.0.

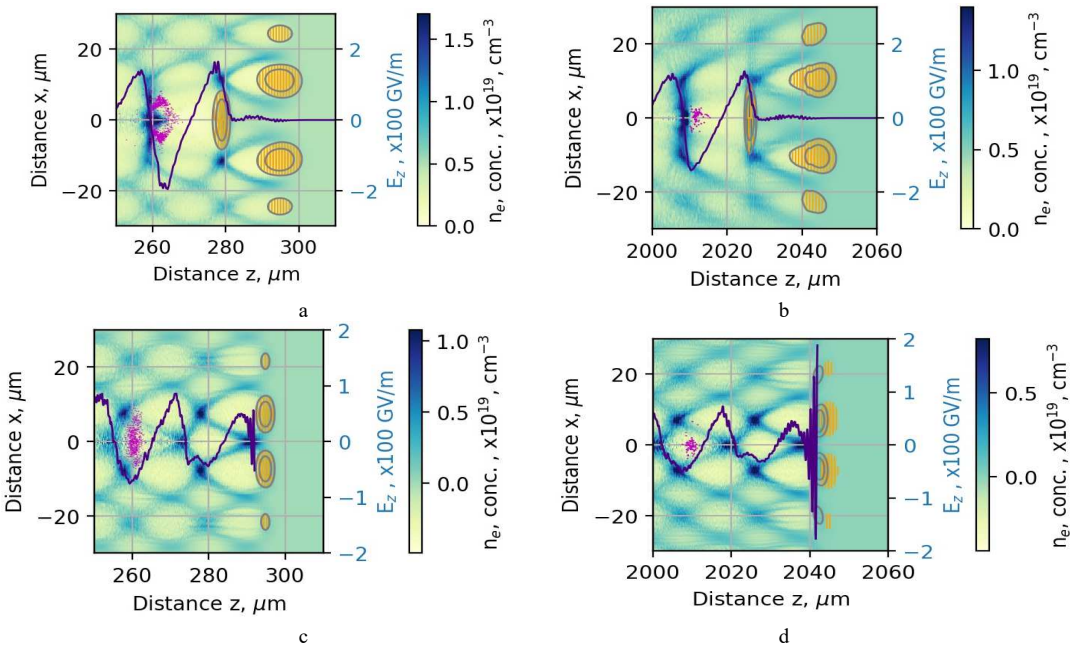

Fig. 10. Distribution of plasma concentration (colour map) and dependence of longitudinal plasma wake electric field E_z (line) formed behind the Gaussian beam with a_0=5.0 guided by the B_1G beam with a_0=1.5 (a, c) and the B_1G beam with a_0=1.9 (c,d) on the acceleration distance. Isolines with yellow oscillating lines represent the location and intensity of the electrical field of the laser pulses. The violet cloud is the electron bunch injected behind the laser pulse.

A Gaussian pulse located behind the B_1G pulse within a ring of high electron concentration (waveguide) (Fig. 10a,b) produces a wake with a strong longitudinal electrical field (line) able to accelerate electron bunch (violet cloud) injected in front of the wake. In addition to electron acceleration, we see a concentration of the bunch closer to the beam propagation axis, which means a reduction in electron bunch divergence.

If only the Bessel-Gauss beam is applied, better acceleration results can be expected when the electron bunch is injected in front of the second wake behind the BG pulse (Fig. 10c,d).

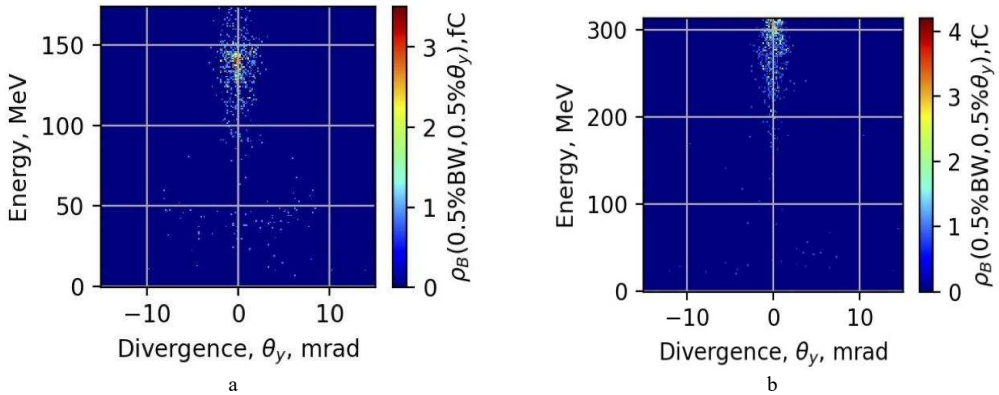

Fig. 11. Energy and divergence θ_y of electrons accelerated by the B_1G beam with a_0=1.9 (a), and the Gaussian beam with the laser strength parameter a_0=5.0, guided by the B_2G beam with a_0=1.5 (b) at the acceleration distance of 2 mm.

The high-energy electron bunches with a moderate energy spread and low divergence could be produced combining guiding the Gaussian accelerating pulse by the doughnut-shaped second-order Bessel-Gauss pulse.

Table 1. Characteristics of the accelerated 1 pC electron bunch using Gaussian and Bessel-Gauss B_1G, B_2G beams in plasma with a concentration of 3×10^{18} cm^{-3} at the distance of 2 mm.

	Driving beam	Guiding beam	a_0 of Driving beam	a_0 of Guiding beam	Pulse duration of Driving beam, fs	Pulse duration of Guiding beam, fs	Weighted average energy of electrons, MeV	Standard deviation of electron energy, MeV	Divergence of electron bunch θ_E, mrad
1.	Gauss	-	1.9	-	10	-	28	7	41
2.	Gauss	-	3.0	-	10	-	47	8	8
3.	Gauss	-	6.5	-	10	-	159	44	27
4.	Gauss	Bessel-Gauss B_2G	5.0	1.5	10	25	244	83	27
5.	Bessel-Gauss B_1G	-	1.3	-	10	-	38	20	46
6.	Bessel-Gauss B_1G	-	1.9	-	10	-	121	38	23
7.	Bessel-Gauss B_1G	-	3.0	-	10	-	149	42	21
8.	Bessel-Gauss B_1G	-	5.0	-	10	-	141	25	23

4. Conclusions

The Gaussian beam at the acceleration distance of 2 mm in the plasma concentration of $n_0= 3\times10^{18}$ cm^{-3} diffracts substantially, and the waist radius of the laser beam increases from 7 μm to 50 μm for $a_0 = 1.9$ and to 24 μm for $a_0 = 6.5$. The guiding of the Gaussian beam with $a_0 = 5.0$ by the B_2G beam with $a_0 = 1.5$ increases the propagation distance. The electric field of the laser beam and longitudinal field of the plasma wake at 2 mm are correspondingly by factors of 2.1 and 2.6 higher relative to the Gaussian beam with $a_0 = 6.5$. The accelerated electrons reach a 53% higher energy of 244±83 MeV with the divergence θ_E =27 mrad.

The kHz class laser pulse energy of 40-60 mJ focused to the waist with a radius of 7-8 μm allows it to reach the intensities of a_0=1.5-2 only. Using a first-order Bessel-Gauss (B_1G) beam having an axial longitudinal electric field, the electrons can be accelerated to 3-4 times higher energy relative to the Gaussian beam with the same laser strength parameter a_0. At the distance of 2 mm, the electrons accelerated by the B_1G beam with $a_0 = 1.9$ reach the energy of 121±38 MeV with θ_E =27 mrad.

5. Methods

For numerical simulation, two open-source Particle-in-cell simulation tools, Wake-T[32] and FBPIC[33], were used. The 3D code Wake-T uses 2D cylindrical geometry (r, z) and quasi-static approximation[34]. The laser pulse evolution was modelled by solving the equation of the vector potential of the envelope[35] rather than simulating the laser wave field. It is, therefore, not necessary to comply with the strict limitation on the simulation step size of the temporal coordinate resulting from the Courant condition. The step size is not limited by the laser wavelength scale; the limitation is only due to the plasma wavelength and Rayleigh length, which are much larger than the laser wavelength. Therefore, the computational efficiency of a quasi-static code can be up to six orders of magnitude higher than a standard 4D PIC code[32]. When simulating beam guiding with Wake-T, the limitation in BG pulse description is that the 2D cylindrical geometry does not allow the introduction of the spiral phase of a high-order BG beam. Therefore, in this work, the results presented by Wake-T are obtained when the BG pulse profile fits the amplitude of the envelope function without the helical phase and propagates without modifications due to diffraction or interaction with the plasma.

The assumption that the BG pulse propagates while maintaining a constant spatial and temporal profile is only valid for a certain propagation distance. Therefore, the quasi-3D FBPIC code, which uses a cylindrical geometry with azimuthal modal decomposition to describe fully the spatial-temporal evolution of the laser beam, was further used to simulate the evolution of the BG pulse and the influence of that evolution on particle acceleration. For the near-cylindrical geometry, only several azimuthal modes are sufficient for beam simulation, making the quasi-3D code much faster than the standard 4D PIC code. The performed test simulation results show that the inclusion of 3 to 5 azimuthal modes is sufficient to model the first and second-order BG beams with a spiral phase.

The simulations were performed for various amplitudes and durations of the Gaussian and BG pulses, both pulses together, separately for Gaussian, and separately for BG pulses. Both pulses had a Gaussian temporal envelope. The size of the coordinate window moving at the speed of light c, $r \times z$ = 180×60 μm^2 was chosen such that in the beam propagation direction (z-axis), it covered both laser pulses and at least two periods of the plasma wave, and along the orthogonal r-coordinate, it was 20÷25 times wider than the width of the first ring of the doughnut BG beam. Open-type boundary conditions at the edges of the coordinate window were used to avoid artificial reflection. The number of nodes in the coordinate grid was 600×600. The number of macroparticles per cell for the Gaussian and the first-order BG beams was (3,3,4), and the number of azimuthal modes was m=3. The number of macroparticles for the second-order Bessel beams was (4,4,5) and the number of azimuthal modes m = 5. The width of the Gaussian envelope of the BG beam was 50 times the width of the BG first ring. To avoid interference of Gaussian and BG laser pulses, polarisations of the pulses were set orthogonal. Initial random distribution of particle coordinates and momentum in an injected electron bunch was Gaussian, transverse and longitudinal RMS length was (1 μm, 1 μm), charge 1 pC, initial energy 10 MeV, energy relative scatter 5%, the number of bunch macro-particles 10^3.

The Wake-T code was used to simulate the plasma structures formed by the BG beam and the Gaussian pulse guiding properties in the BG plasma wake. The FBPIC code was used to model the electron bunch acceleration by the Gaussian pulse and Gaussian pulse guided in the BG plasma wake and acceleration of an electron bunch using only the BG pulse.

Laser beam/pulse configurations used in the research:

1. Gaussian beam (G);
2. Bessel-Gauss beam (BG) - doughnut-shaped, first or second-order optical vortex;
3. The first-order Bessel-Gauss beam (pulse), followed by a Gauss pulse (G+B$_1$G);
4. The second-order Bessel-Gauss beam (pulse), followed by a Gauss pulse (G+B$_2$G).

The Gaussian or Bessel-Gauss beam or pulse in the article means transversal energy distribution in the laser pulse, while the temporal shape of the pulse is assumed to be Gaussian.

A 2D cylindrical quasi-static PIC code Wake-T[32] was used to simulate the accelerating laser pulse propagation in a plasma channel generated by a Bessel-Gauss beam. The envelope of the normalised vector potential of the linear-polarised n_{th}-order BG beam had the shape

$$a_b(r,\varphi,\eta) = a_{ob} J_n(\rho r)\, exp\left(-\frac{r^2}{w_{0b}^2} - (\frac{\eta}{c\tau_b})^2 + in\varphi\right), \quad (1)$$

where

$$a_{0b} = \frac{eA_b}{m_e c^2} \quad (2)$$

is the amplitude of the normalised vector potential, also called the laser strength parameter; J_n is the n_{th}-order Bessel function (n=1, 2); $w_b = r_n/\rho$ is the distance from the axis of the Bessel beam to the first ring, and for the n=1, the constant is r_n=1.84, for the n=2, r_n =3; w_{0b} is the Gaussian envelope radius of the Bessel-Gauss (BG) beam; $\eta = z - ct - z_{cb}$ is the longitudinal coordinate in the moving coordinate window; z_{cb} is the pulse peak coordinate; τ_b is the pulse duration of the BG beam; r, φ is the radial, azimuthal coordinate. In the Wake-T modelling of the BG beam propagation in plasma, it was assumed that there is no dependency on azimuthal coordinate and the envelope of the vector potential is preserved.

The driving pulse envelope of the normalised vector potential with the linear polarisation, orthogonal to the polarisation of the BG beam, had the Gaussian temporal and spatial shape

$$a(r,\eta) = a_o \exp\left(-\frac{r^2}{w_0^2} - (\frac{\eta}{c\tau_b})^2 \right) \quad (3)$$

Here a_0 is the amplitude of the normalised vector potential, also called the laser strength parameter; w_0 is the radius of the beam; $\eta = z - ct - z_c$ is the longitudinal coordinate in the moving coordinate window; z_c is the pulse peak coordinates; τ is the pulse duration.

Funding. The research leading to these results was funded by the Research Council of Lithuania under grant agreement No. S-MIP-21-3.

Author's Contributions V. Girdauskas performed the physical analysis, defined the methodology, carried out the Wake-T and FBPIC simulation, and wrote the original draft. V. Tomkus carried out the physical analysis and FBPIC simulation, and wrote the original draft. M. Abedi-Varaki worked on the physical analysis and FBPIC simulation, and wrote the original draft. G. Raciukaitis: defined the methodology, supervised the research, conceived and defined the aims of the investigation, reviewed and edited the manuscript. All authors reviewed the obtained results and commented on the paper.

Competing interests The authors declare no competing interests.

Ethics Approval This paper has not been submitted for publication elsewhere. We further certify that proper citations to the previously reported work have been given and no data/tables/figures have been quoted verbatim from other publications without giving due acknowledgement and without the permission of the author(s).

Data Availability The authors confirm that all of the data and codes used in this study are available from the corresponding author on reasonable request.

References

1. Hansen, S. *et al.* Measurement of 2l− nl′ x-ray transitions from≈ 1 μ m Kr clusters irradiated by high-intensity femtosecond laser pulses. *Physical Review E* **71**, 016408 (2005).
2. Fukuda, Y. *et al.* Optimized energetic particle emissions from Xe clusters in intense laser fields. *Physical Review A* **67**, 061201 (2003).
3. Jianjun, L. *et al.* in *2015 IEEE International Conference on Plasma Sciences (ICOPS).* http://stacks.iop.org/1882-0786/9/i=6/a=062003 (2016).
4. Milchberg, H., Kim, K., Kumarappan, V., Layer, B. & Sheng, H. Clustered gases as a medium for efficient plasma waveguide generation. *Philosophical Transactions of the Royal Society A: Mathematical, Physical and Engineering Sciences* **364**, 647-661 (2006).
5. Daigle, J.-F. *et al.* Long range trace detection in aqueous aerosol using remote filament-induced breakdown spectroscopy. *Applied Physics B* **87**, 749-754 (2007).
6. Stelmaszczyk, K. *et al.* Long-distance remote laser-induced breakdown spectroscopy using filamentation in air. *Applied Physics Letters* **85**, 3977-3979 (2004).
7. Liu, J., Dai, J., Chin, S. L. & Zhang, X.-C. Broadband terahertz wave remote sensing using coherent manipulation of fluorescence from asymmetrically ionized gases. *Nature Photonics* **4**, 627-631 (2010).
8. Kim, K.-Y., Taylor, A., Glownia, J. & Rodriguez, G. Coherent control of terahertz supercontinuum generation in ultrafast laser–gas interactions. *Nature Photonics* **2**, 605-609 (2008).
9. Singh, A. & Gupta, N. Higher harmonic generation by self-focused q-Gaussian laser beam in preformed collisionless plasma channel. *Laser and Particle Beams* **32**, 621-629 (2014).
10. Oliva, E. *et al.* 3D multi-scale modelling of plasma-based seeded soft X-ray lasers. *The European Physical Journal D* **75**, 1-8 (2021).

11. Esarey, E., Schroeder, C. & Leemans, W. Physics of laser-driven plasma-based electron accelerators. *Reviews of modern physics* **81**, 1229 (2009).
12. Leemans, W. *et al.* Multi-GeV electron beams from capillary-discharge-guided subpetawatt laser pulses in the self-trapping regime. *Physical review letters* **113**, 245002 (2014).
13. Gonsalves, A. *et al.* Petawatt laser guiding and electron beam acceleration to 8 GeV in a laser-heated capillary discharge waveguide. *Physical review letters* **122**, 084801 (2019).
14. Shalloo, R. *et al.* Low-density hydrodynamic optical-field-ionized plasma channels generated with an axicon lens. *Physical Review Accelerators and Beams* **22**, 041302 (2019).
15. Tzortzakis, S., Prade, B., Franco, M. & Mysyrowicz, A. Time-evolution of the plasma channel at the trail of a self-guided IR femtosecond laser pulse in air. *Optics communications* **181**, 123-127 (2000).
16. Hao, Z. *et al.* Prolongation of the fluorescence lifetime of plasma channels in air induced by femtosecond laser pulses. *Applied Physics B* **80**, 627-630 (2005).
17. Mohamed, W. T. *et al.* Controlling the length of plasma waveguide up to 5 mm, produced by femtosecond laser pulses in atomic clustered gas. *Optics Express* **19**, 15919-15928 (2011).
18. Lu, X. *et al.* Quasi-steady-state air plasma channel produced by a femtosecond laser pulse sequence. *Scientific reports* **5**, 1-9 (2015).
19. Smartsev, S. *et al.* Axiparabola: a long-focal-depth, high-resolution mirror for broadband high-intensity lasers. *Optics letters* **44**, 3414-3417 (2019).
20. Shalloo, R. *et al.* Hydrodynamic optical-field-ionized plasma channels. *Physical Review E* **97**, 053203 (2018).
21. Lemos, N. *et al.* Guiding of laser pulses in plasma waveguides created by linearly-polarized femtosecond laser pulses. *Scientific reports* **8**, 1-9 (2018).
22. Zhang, G.-B. *et al.* Acceleration of on-axis and ring-shaped electron beams in wakefields driven by Laguerre-Gaussian pulses. *Journal of Applied Physics* **119**, 103101 (2016).
23. Tang, R.-A. *et al.* Propagation dynamics of an azimuthally polarized Bessel–Gauss laser beam in a parabolic plasma channel. *Physics of Plasmas* **27**, 113103 (2020).
24. Vieira, J. & Mendonça, J. Nonlinear laser driven donut wakefields for positron and electron acceleration. *Physical review letters* **112**, 215001 (2014).
25. Osterhoff, J. *et al.* Generation of stable, low-divergence electron beams by laser-wakefield acceleration in a steady-state-flow gas cell. *Physical review letters* **101**, 085002 (2008).
26. Geddes, C. *et al.* Plasma-density-gradient injection of low absolute-momentum-spread electron bunches. *Physical review letters* **100**, 215004 (2008).
27. Budriūnas, R. *et al.* 53 W average power CEP-stabilized OPCPA system delivering 5.5 TW few cycle pulses at 1 kHz repetition rate. *Optics Express* **25**, 5797-5806 (2017).
28. Faure, J. *et al.* A review of recent progress on laser-plasma acceleration at kHz repetition rate. *Plasma physics and controlled fusion* **61**, 014012 (2018).
29. Fuchs, T. *et al.* Treatment planning for laser-accelerated very-high energy electrons. *Physics in Medicine & Biology* **54**, 3315 (2009).
30. Subiel, A. *et al.* Challenges of dosimetry of ultra-short pulsed very high energy electron beams. *Physica Medica* **42**, 327-331 (2017).
31. Kokurewicz, K. *et al.* Focused very high-energy electron beams as a novel radiotherapy modality for producing high-dose volumetric elements. *Scientific reports* **9**, 1-10 (2019).
32. Pousa, A. F., Aßmann, R. & de la Ossa, A. M. in *Journal of Physics: Conference Series* **1350***,* 012056 (2019)(.
33. Lehe, R., Kirchen, M., Andriyash, I. A., Godfrey, B. B. & Vay, J.-L. A spectral, quasi-cylindrical and dispersion-free Particle-In-Cell algorithm. *Computer Physics Communications* **203**, 66-82 (2016).
34. Pukhov, A. Particle-in-cell codes for plasma-based particle acceleration. *arXiv preprint https://arxiv.org/abs/1510.01071*(2015).
35. Benedetti, C., Schroeder, C., Geddes, C., Esarey, E. & Leemans, W. An accurate and efficient laser-envelope solver for the modeling of laser-plasma accelerators. *Plasma physics and controlled fusion* **60**, 014002 (2017).

Fig. 1. Electron charge density distribution $\rho(r, \eta)$ in BG created plasma wave (green-blue) and the first-order BG pulse envelope (isolines). Dotted lines mark the positions of longitudinal and transverse cross-sections of charge density profiles shown in Fig. 2 and Fig. 3. Plasma electron concentration $n0=3\times10^{18}cm^{-3}$, BG pulse parameters: a_{0b}=1.5, τ_b=25 fs, w_{0b}=7.5 μm. The laser pulse propagates from the left to right side along the z-axis, centred at r=0.

Fig. 2 Transverse profiles of electron charge density $\rho(r)$ for first-order (a) and second-order (b) BG pulses and various values of the laser strength parameter a_{0b}. The green line in (a) is a parabolic approximation. Plasma electron concentration $n_0=3\times10^{18}cm^{-3}$, BG pulse parameters: τ_b=25 fs, w_{0b}=7.5 μm.

Fig. 3. Longitudinal profiles of the electron charge density ρ (η) for various laser strength parameter values a0b of the BG pulse (solid lines) and normalised envelopes of the accelerating Gaussian (green) and BG pulses (yellow). Plasma electron concentration $n_0=3\times10^{18}cm^{-3}$; Gaussian pulse duration τ=10 fs; BG pulse parameters: τ_b=25 fs, w_{0b}=7.5 μm.

Fig. 4. Dependence of the maximum charge density in the ring-shaped electron plasma wave created by the BG laser pulse on its duration for two different initial plasma electron concentrations: $n_0=1\times10^{18}cm^{-3}$, $n_0=3\times10^{18}cm^{-3}$. BG pulse parameters: a_{0b}=1.5, τ_b=25 fs, w_{0b}=7.5 μm.

Fig. 5. Electron charge density distribution $\rho(r, \eta)$ in the plasma wave (green-blue) and the envelopes (isolines) of the accelerating Gaussian pulse and pulses of B_1G (a) B_2G (b) beams. Parameters of the accelerating Gaussian and BG pulses: a_0=2.0, τ=10 fs, w_0=7 μm, a_{0b}=1.5, τ_b=25 fs, w_{0b}=7.5 μm (a); w_{0b}=11 μm (b).

Fig. 6. Transverse profiles $a(r)$ of the accelerating pulse amplitude at the pulse peak, guided by the first-order (a) and second-order (b) BG pulses at various propagation distances in plasma (0, 1, 2, 3 mm). Parameters of the accelerating Gaussian and BG pulses: a_0=2.0, τ=10 fs, w_0=7 μm, a_{0b}=1.5, τ_b=25 fs, w_{0b}=7.5 μm.

Fig. 7. Dependence of the energy of accelerated electrons (a), energy spread σ_{En} (b), divergence θ_E (c), and driver pulse amplitude (d) on the acceleration distance for Gaussian (G), Gaussian and B_2G (G+B_2G), Gaussian and B_1G (G+B_1G) and B_1G (B_1G) laser beams. Parameters of the accelerating Gaussian and Bessel-Gauss beams: τ=10 fs, w_0=7 μm, a_{0b}=1.5, τ_b=25 fs, w_{0b}=7.5 μm and a_{0b}=1.3 for B_1G, w_{0b}=11 μm and a_{0b}=1.5 for B_2G, a_0=6 for G; a_0=5 for G+B_2G, a_0=1.5 for G+B_1G.

Fig. 8. Dependence of the longitudinal plasma wake electric field E_z (solid line) and the electric field of laser beam envelope (dotted line) for acceleration distances 0.25 mm, 0.5 mm, 1 mm, 2 mm of the Gaussian beam with the laser strength parameter a_0=1.9 (a), a_0=3.0 (b), a_0=6.5 (c) and the Gaussian beam with a_0=5.0 guided by the B_2G beam with a_0=1.5 (G+B_2G) (d).

Fig. 9. Distribution of plasma concentration (colour map) and longitudinal plasma wake electric field E_z (line) formed along a beam axis by the Gaussian beam with the laser strength parameter a_0=1.9 (a,b) and a_0=6.5 (c,d). Isolines and yellow oscillating lines represent the location and intensity of the electrical field of the laser pulse. The violet cloud is the electron bunch injected behind the laser pulse.

Fig. 10. Distribution of plasma concentration (colour map) and dependence of longitudinal plasma wake electric field E_z (line) formed behind the Gaussian beam with a_0=5.0 guided by the B_1G beam with a_0=1.5 (a, c) and the B_1G beam with a_0=1.9 (c,d) on the acceleration distance. Isolines with yellow oscillating lines represent the location and intensity of the electrical field of the laser pulses. The violet cloud is the electron bunch injected behind the laser pulse.

Fig. 11. Energy and divergence θ_y of electrons accelerated by the B_1G beam with a_0=1.9 (a), and the Gaussian beam with the laser strength parameter a_0=5.0, guided by the B_2G beam with a_0=1.5 (b) at the acceleration distance of 2 mm.

Table 1. Characteristics of the accelerated 1 pC electron bunch using Gaussian and Bessel-Gauss B_1G, B_2G beams in plasma with a concentration of 3×10^{18} cm^{-3} at the distance of 2 mm.